## **RSC Advances**



PAPER

View Article Online

View Journal | View Issue



Cite this: RSC Adv., 2018, 8, 2092

# Synthesis and characterisation of brannerite compositions ( $U_{0.9}Ce_{0.1}$ )<sub>1-x</sub> $M_xTi_2O_6$ ( $M=Gd^{3+}$ , $Ca^{2+}$ ) for the immobilisation of MOX residues

D. J. Bailey, 🕩 \*a M. C. Stennett, 🕩 B. Ravel, b D. Grolimund c and N. C. Hyatta

A suite of uranium brannerites for the disposal of MOX residues, formulated ( $U_{0.9}Ce_{0.1}$ )<sub>1-x</sub> $M_xTi_2O_6$  ( $M=Ca^{2+}$  and/or  $Gd^{3+}$ ), were prepared using a mixed oxide route under oxidising, inert and reducing atmospheres (air, argon and  $H_2/N_2$ ).  $Gd^{3+}$  was added to act as a neutron absorber in the final Pu bearing wasteform and Ce added to function as a structural analogue for Pu. X-ray powder diffraction of the synthesised specimens found that phase distribution was strongly affected by the processing atmosphere and Gd content. In all cases prototypical brannerite was formed, accompanied by different secondary phases dependent on processing atmosphere. Microstructural analysis (SEM) of the sintered samples confirmed the results of the X-ray powder diffraction. Bulk XANES found that Ti remained in the  $Ti^{4+}$  oxidation state whereas Ti0 ce was uniformly reduced to the Ti1 condition of Ti2 oxidation states to charge compensate. It was concluded that the charge balance mechanism was a combination of Ti3 oxidation and Ti3 oxidation and Ti3 oxidation and Ti4 oxidation and Ti5 oxidation and Ti6 oxidation and Ti7 oxidation and Ti8 oxidation and T

Received 24th October 2017 Accepted 21st December 2017

DOI: 10.1039/c7ra11742f

rsc.li/rsc-advances

#### 1 Introduction

Separated plutonium stockpiles, accumulated as a result of the continued reprocessing of spent nuclear fuel (SNF),¹ present an ongoing challenge in terms of their safe, long-term management and also a potential proliferation risk.² Consequently, reduction of accumulated stockpiles is highly desirable. Re-use of Pu in mixed oxide fuel (MOX), is an option currently favoured by the UK government.¹ During production of mixed oxide fuels, residues rich in Pu and U are generated. Although the majority of MOX residues can be recycled and reused to make fuel, it is inevitable that some fraction will be uneconomic to recycle and will require immobilisation and disposal.

Brannerite (UTi $_2O_6 \sim 55$  wt% U) is a titanate phase commonly found in uranium ore deposits<sup>3</sup> and as an accessory phase in zirconolite and pyrochlore based ceramics designed for actinide disposition. <sup>4,5</sup> Brannerite has a monoclinic crystal structure with space group C2/m, comprising layers of edge sharing TiO $_6$  octahedra linked by octahedra with larger cations (U). <sup>6</sup> Naturally occurring brannerites exhibit considerable chemical flexibility with elements such as Ca, Y, Pb, Ce and Th being incorporated on the U site and Fe, Si and Al substituting on the Ti site. However, they are commonly completely

metamict due to accumulated  $\alpha$ -recoil damage (critical dose 1–3  $\times$  10<sup>16</sup>  $\alpha$  mg<sup>-1</sup>).<sup>3,7</sup> Nevertheless, the presence of brannerite as a heavy mineral in alluvial sediments, after the host rock has been weathered, provides an indication of the long term durability of brannerite.<sup>8</sup> Previous studies have shown that it is possible to synthesise Pu-bearing brannerites and also that the Pu analogue, Ce, adopts the brannerite structure.<sup>4,9</sup> The production of a Pu-bearing wasteform may require the incorporation of neutron absorbing species, such as Gd or Hf, for criticality safety; these have been shown to form brannerite solid solutions with Pu by Vance *et al.*<sup>4</sup>

The synthesis of stoichiometric brannerite requires inert conditions.<sup>10</sup> However, it is possible to stabilize the brannerite structure in air by the addition of dopants (Ca, La, Gd).<sup>4,5,11-13</sup> This indicates that both processing conditions and target stoichiometry may affect brannerite formation.

In this study, the production of brannerites suitable for MOX disposal was investigated by synthesising brannerites with a range of conceptual waste loadings  $((U_{0.9}Ce_{0.1})_{1-x}M_xTi_2O_6)$  under different atmospheres in an attempt to find a suitable baseline composition and processing conditions.

#### 2 Materials and methods

#### 2.1 Materials synthesis

Four different compositions of brannerite  $(Gd_{0.1}U_{0.81}Ce_{0.09}Ti_2-O_6, Gd_{0.2}U_{0.72}Ce_{0.08}Ti_2O_6, Gd_{0.25}U_{0.675}Ce_{0.075}Ti_2O_6$  and  $Ca_{0.1}-Gd_{0.1}U_{0.72}Ce_{0.08}Ti_2O_6)$  were synthesised by solid state reaction of component oxides and  $CaCO_3$  under oxidising, inert and

<sup>&</sup>quot;Immobilisation Science Laboratory, Department of Materials Science and Engineering, University of Sheffield, UK. E-mail: d.j.bailey@sheffield.ac.uk

<sup>&</sup>lt;sup>b</sup>National Institute of Standards and Technology, 100 Bureau Drive, Gaithersburg, MD 20899, USA

Swiss Light Source, Paul Scherrer Institute, Villigen 5232, Switzerland

Paper RSC Advances

reducing atmospheres (air, argon and 5%  $H_2/N_2$ ). Gd was added to act as a neutron absorber in a final Pu-bearing wasteform and to stabilise higher U oxidation states ( $U^{5+/6+}$ ) in the brannerite structure by charge compensation (see below). Ce was used as a structural analogue for plutonium. MOX fuel compositions for light water reactors are envisaged to contain 5–10% Pu therefore the atomic ratio of U to Ce was maintained at 9:1 in all compositions as an approximation of the upper bounds of expected MOX fuel composition. Charge balancing of diand trivalent cations ( $Ca^{2+}$  and  $Gd^{3+}$ ) was expected to occur via the oxidation of  $U^{4+}$  to higher oxidation states ( $U^{5+}$ ,  $U^{6+}$ ) as observed in previous studies.

Reagents (UO<sub>2</sub>, CeO<sub>2</sub>, Gd<sub>2</sub>O<sub>3</sub>, TiO<sub>2</sub> and CaCO<sub>3</sub>) were mixed with isopropanol to form a slurry and ball milled for five minutes at a frequency of 30 Hz using a Fritsch Pulverisette 23. The milled slurry was dried in an oven (95  $^{\circ}$ C) and a sample from each composition ( $\sim$ 0.6 g) reacted at 1300  $^{\circ}$ C for 12 hours under flowing air, argon or 5% H<sub>2</sub>/N<sub>2</sub>.

Sintered pellets were produced by uniaxially pressing reacted powders in a hardened steel die (6 mm diameter) and sintering under atmosphere (argon, air,  $5\% \text{ H}_2/\text{N}_2$ ) at  $1320 \,^{\circ}\text{C}$  for 12 hours.

#### 2.2 Materials characterisation

Reacted powders were ground and characterised by powder X-ray diffraction with a Bruker D2 Phaser X-ray diffractometer using Cu K $\alpha$  radiation. Cu K $\beta$  radiation was filtered using a Ni foil. XRD data were processed using the Bruker DiffracEva software package.

Sintered pellets were characterised by scanning electron microscopy and energy dispersive X-ray spectroscopy (SEM-EDX) using a Hitachi TM3030 SEM equipped with a Bruker Quantax EDX. An accelerating voltage of 15 kV was used for imaging. EDX data were analysed using Bruker Quantax software. Sintered pellets were prepared for SEM analysis by mounting in cold setting resin and polishing with SiC paper and progressively finer diamond pastes to an optical finish (1  $\mu m$ ). Samples were sputter coated with carbon to reduce surface charging effects.

#### 2.3 X-ray absorption near edge spectroscopy

Samples were characterised using X-ray absorption near edge spectroscopy (XANES) to determine the average oxidation state of U, Ce and Ti. Samples were investigated at the Ti K-edge (4966 eV), Ce L-III edge (5723 eV) and U L-III edge (17 166 eV) using a conventional XAS setup at the now decommissioned beamline X23A2, National Synchrotron Lightsource, Brookhaven National Laboratory. Samples were prepared for XAS analysis by homogenously mixing ground, reacted powders with polyethylene glycol and uniaxially pressing to form 13 mm diameter pellets of approximately one absorption length.

Samples were measured alongside standards of known oxidation states to allow the derivation of the average oxidation state of the element of interest. Ti and Ce edges were measured in fluorescence mode. Ti measurements were made alongside Ti<sup>4+</sup>, Ti<sup>3+</sup>, Ti<sup>2+</sup> and Ti<sup>(0)</sup> standards (TiO<sub>2</sub>, Ti<sub>2</sub>O<sub>3</sub>, TiO and Ti metal foil respectively) and Ce measurements were made alongside Ce<sup>3+</sup> and Ce<sup>4+</sup> standards (CePO<sub>4</sub> and CeO<sub>2</sub> respectively). The U L-III edge was

measured in transmission alongside  $U^{4+}$ ,  $U^{5+}$  and  $U^{6+}$  standards: brannerite ( $U^{4+}$ – $UTi_2O_6$ ), mixed brannerite ( $U^{5+}$ – $Y_{0.5}U_{0.5}Ti_2O_6$ ) and calcium uranate ( $U^{6+}$ – $CaUO_4$ ).  $Y_{0.5}U_{0.5}Ti_2O_6$  was produced according to the method described by James *et al.*<sup>11</sup> The edge position was determined to be the maximum of the first derivative of the absorption spectrum, the average U oxidation state was determined by performing a linear regression of first derivative energies with respect to standards of known oxidation state.

Incident  $(I_0)$  and transmitted  $(I_t)$  X-ray intensities were measured using ion chambers, energy calibration was performed using XANES spectra measured with a reference ion chamber  $(I_r)$  of a standard placed after the transmission ion chamber in the beam path. Fluorescence mode measurements were made using a four element vortex Si-drift detector. XANES spectra were measured from 30 eV below the edge of interest to 250 eV above. A Si (311) monochromator was used to tune the energy of incident photons giving an energy resolution of  $\pm 0.3$  eV. Data reduction and XANES analysis were performed using the program Athena. <sup>15,16</sup>

#### 2.4 Micro-focus X-ray absorption spectroscopy

To determine the U oxidation state exclusively in the brannerite phase, in the presence of accessory phases, samples were studied using micro-focus X-ray absorption spectroscopy at beamline X05LA, Swiss Light Source, Paul Scherrer Institute, Switzerland. Samples were mounted in cold setting resin before being thin-sectioned and mounted on a Spectrasil slide. For measurement, samples were mounted on a motorised x-y-z stage to allow scanning of the sample in the beam and a spot size of approximately 1  $\mu$ m<sup>2</sup> was used.

To aid in the selection of regions of interest, 30 μm<sup>2</sup> fluorescence maps were produced by rastering the sample in the beam at an energy of 17 200 eV. X-ray fluorescence was measured using a Si drift detector (KETEK) mounted 45° to the incident beam. XRF maps were produced by windowing specific regions of the fluorescence spectrum corresponding to the emission lines of U, Gd and Ti. Points of interest for XANES study were then selected on the basis of relative intensities of Gd, Ti and U and knowledge of the respective phase assemblages and elemental partitioning of the samples from prior SEM-EDX analysis. Multiple XANES spectra per sample were measured from 30 eV below the U L-III edge to 250 eV above and then averaged, photon energy was tuned using a double crystal Si (111) monochromator. Again, data reduction and XANES analysis were performed using the program Athena. 15,16 The average uranium oxidation state in the brannerite phase was determined by performing linear regression of the energy value at half the edge step with respect to standards of known oxidation state.

#### 3 Results and discussion

#### 3.1 Powder X-ray diffraction

All samples produced were characterised by powder X-ray diffraction and sharp reflections indicative of prototypical brannerite were observed in all cases. Other, secondary phases, were observed dependent on processing atmosphere and

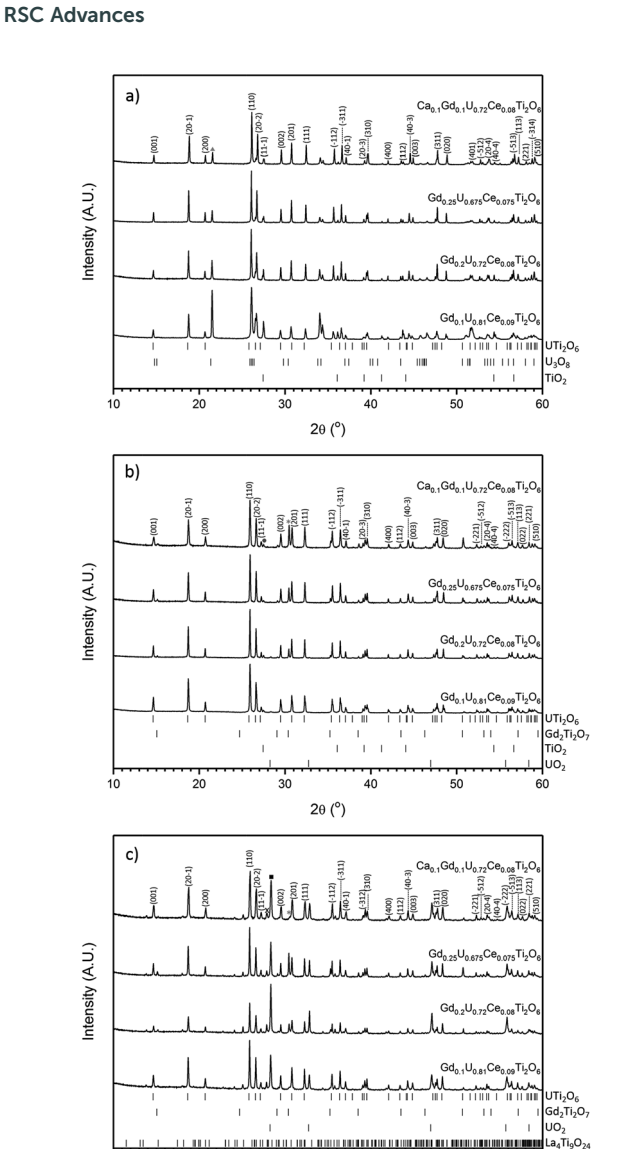


Fig. 1 Powder X-ray diffraction results for compositions sintered under atmosphere: (a) air, (b) Ar and (c) 5%  $H_2/N_2$ . Major reflections of secondary phases are indicated by symbols: Triangle- $U_3O_8$ ; Circle- $TiO_2$  (rutile); Square- $UO_2$ ; Asterisk- $Gd_2Ti_2O_7$  and X-La<sub>4</sub> $Ti_9O_{24}$ . Reference patterns were obtained from the ICSD database (UTi<sub>2</sub>O<sub>6</sub>-ICSD 201342,  $Gd_2Ti_2O_7$ -ICSD 167918,  $U_3O_8$ -ICSD 28137,  $TiO_2$  (rutile)-ICSD 33837,  $UO_2$ -ICSD 246851, La<sub>4</sub> $Ti_9O_{24}$ -ICSD 80052).

20 (°)

composition. Samples sintered in air contained three phases: brannerite,  $U_3O_8$  and rutile (TiO<sub>2</sub>); these results are in agreement with those reported by previous studies.<sup>4,5,10,12,13</sup> As can be seen in Fig. 1a, as the level of Gd substitution increased the major peaks associated with  $U_3O_8$  decreased, this indicates that the formation of the brannerite phase in air is stabilised by the addition of Gd.

Samples sintered in Ar were found to contain a mixture of prototypical brannerite, rutile and a pyrochlore phase, see Fig. 1b. Considering the solid solution limits quoted by James and Watson (2002) for brannerites in the series  $Gd_xU_{1-x}Ti_2O_6$  produced under similar conditions, 0 < x < 0.45, these results are unexpected. Unlike samples sintered in air, increased substitution of Gd was seen to have a detrimental effect on the phase assemblage with the relative proportion of the pyrochlore phase showing a concomitant increase.

Samples sintered in 5%  $\rm H_2/N_2$ , see Fig. 1c, were found to contain brannerite,  $\rm UO_2$ , a pyrochlore phase and a rare-earth rich titanate phase related to the  $\rm La_4Ti_9O_{24}$  structure. A similar titanate phase has previously been found to form in  $\rm CeTi_2O_6$  ceramics when sintered in Ar and has also been observed in brannerite-based ceramics by Stefanovksy *et al.* <sup>17</sup> As with samples produced in inert atmospheres, increased substitution of Gd led to an increase in the intensities attributed to the pyrochlore phase.

Although there was not significant variation in unit cell volume between different compositions produced in the same atmosphere; there is clear variation between samples produced in different atmospheres (Table 1). Samples produced in air were found to have the smallest unit cells and those produced in 5%  $H_2/N_2$  the largest. Considering the ionic radii of  $U^{4+}$ ,  $U^{5+}$  and  $U^{6+}$  in octahedral coordination (0.89, 0.76 and 0.73 Å respectively), these results are consistent with the incorporation of more highly oxidised U in samples sintered in air and the retention of  $U^{4+}$  in samples produced in 5%  $H_2/N_2$ .

# 3.2 Scanning electron microscopy-energy dispersive X-ray spectroscopy (SEM-EDX)

Scanning electron microscopy was used to examine the phase distribution in sintered samples. In agreement with XRD data, brannerite was observed in all cases, with differing accessory

Table 1 Refined lattice parameters of synthesised brannerites

Nominal composition	Atmosphere	a (Å)	b (Å)	c (Å)	β (°)	$V(\mathring{\mathbf{A}}^3)$
$Gd_{0.1}U_{0.81}Ce_{0.09}Ti_{2}O_{6}$	Air	9.8172(2)	3.7390(1)	6.9196(2)	118.554(1)	253.997(2)
$Gd_{0.2}U_{0.72}Ce_{0.08}Ti_2O_6$	Air	9.8210(2)	3.7370(1)	6.9101(1)	118.607(1)	253.611(2)
$Gd_{0.25}U_{0.675}Ce_{0.075}Ti_2O_6$	Air	9.8207(1)	3.7371(1)	6.9099(1)	118.607(1)	253.599(1)
$Ca_{0.1}Gd_{0.1}U_{0.72}Ce_{0.08}Ti_2O_6$	Air	9.8145(2)	3.7346(1)	6.9027(1)	118.482(1)	253.007(2)
$Gd_{0.1}U_{0.81}Ce_{0.09}Ti_2O_6$	Ar	9.8192(1)	3.7617(1)	6.9253(1)	118.807(1)	255.802(1)
$Gd_{0.2}U_{0.72}Ce_{0.08}Ti_2O_6$	Ar	9.8215(2)	3.7612(1)	6.9240(1)	118.799(1)	255.779(2)
$Gd_{0.25}U_{0.675}Ce_{0.075}Ti_{2}O_{6}$	Ar	9.8208(2)	3.7510(1)	6.9219(1)	118.797(1)	255.598(2)
$Ca_{0.1}Gd_{0.1}U_{0.72}Ce_{0.08}Ti_2O_6$	Ar	9.8210(6)	3.7660(2)	6.9293(4)	118.825(1)	256.284(6)
$Gd_{0.1}U_{0.81}Ce_{0.09}Ti_2O_6$	$5\% H_2/N_2$	9.8197(2)	3.7695(1)	6.9297(2)	118.864(1)	256.504(2)
$Gd_{0.2}U_{0.72}Ce_{0.08}Ti_2O_6$	$5\% H_2/N_2$	9.8286(5)	3.7702(2)	6.9324(4)	118.867(3)	256.884(5)
$Gd_{0.25}U_{0.675}Ce_{0.075}Ti_2O_6$	$5\% H_2/N_2$	9.8251(3)	3.7686(1)	6.9292(2)	118.867(1)	256.565(3)
$Ca_{0.1}Gd_{0.1}U_{0.72}Ce_{0.08}Ti_2O_6$	$5\% H_2/N_2$	9.8192(2)	3.7693(1)	6.9294(1)	118.867(1)	256.468(2)

Paper

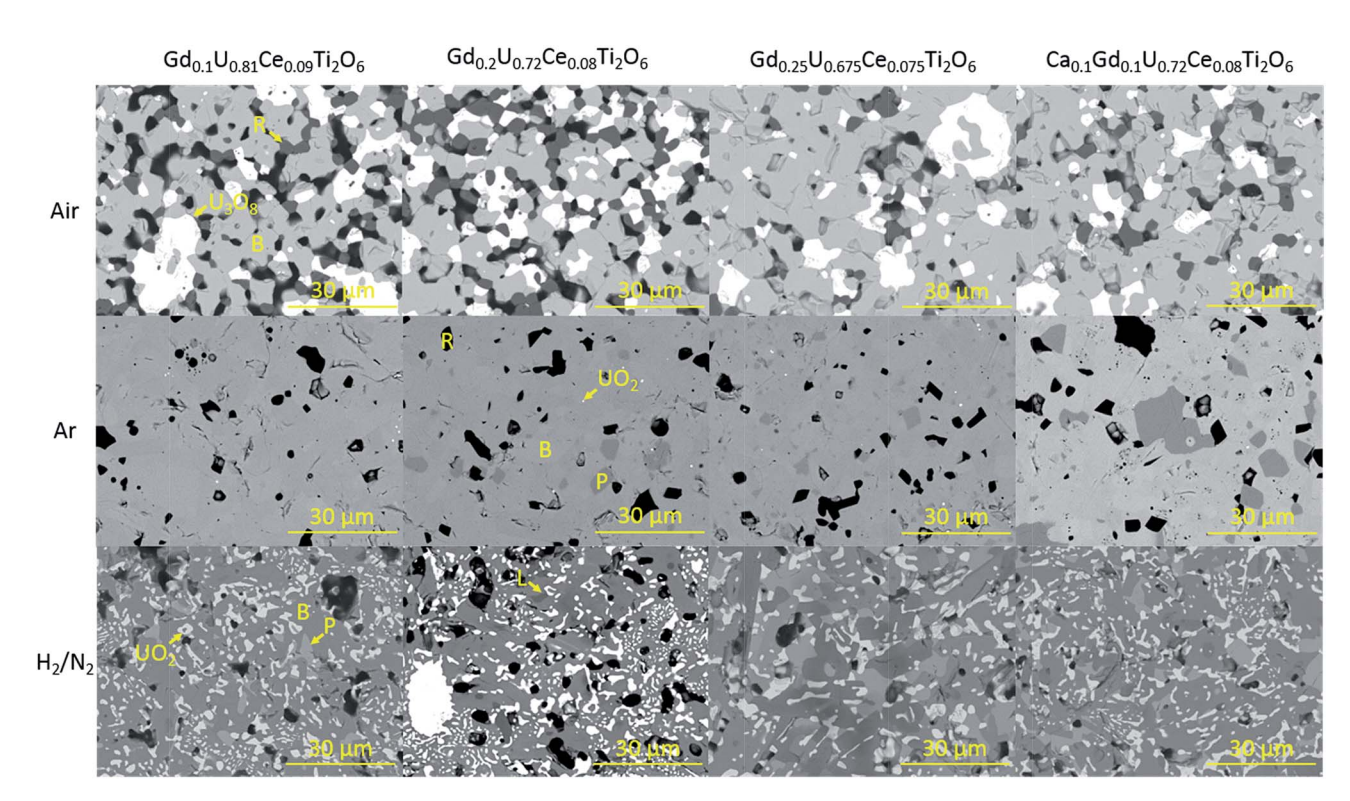


Fig. 2 Representative backscattered electron images of sintered brannerites. B-brannerite, R-rutile, P-pyrochlore, L-Lan<sub>4</sub>Ti<sub>9</sub>O<sub>24</sub>

phases dependent upon processing atmosphere. Representative backscattered electron images of sintered brannerites are shown in Fig. 2.

Three distinct phases were formed when samples were synthesised in air: brannerite,  $U_3O_8$  and rutile (TiO<sub>2</sub>). Significant porosity was observed throughout all compositions, this is in agreement with the porosity observed by Vance *et al.* for samples synthesised under similar conditions.<sup>4</sup>

The phase distribution observed in samples sintered in argon was markedly different to that of samples sintered in air. In agreement with XRD results, there are several phases present within the samples; predominantly brannerite, rutile and

pyrochlore with some retained UO<sub>2</sub>. As can be seen in Fig. 2, although there is no evidence of pyrochlore formation in the  $Gd_{0.1}U_{0.81}Ce_{0.09}Ti_2O_6$  composition, pyrochlore formation was observed for all other compositions. These results are in contrast to those reported by Vance *et al.* and James and Watson who found that substituted Gd formed a solid solution up to a limit of 0.45 formula units when  $Gd_xU_{1-x}Ti_2O_6$  brannerites were produced in an inert atmosphere. Bailey *et al.* found that substitution of Gd in the system  $Gd_xU_{1-x}Ti_2O_6$  led to the formation of a parasitic pyrochlore phase at a substitution level as low as 0.2 formula units, these results are consistent with those presented in this study.

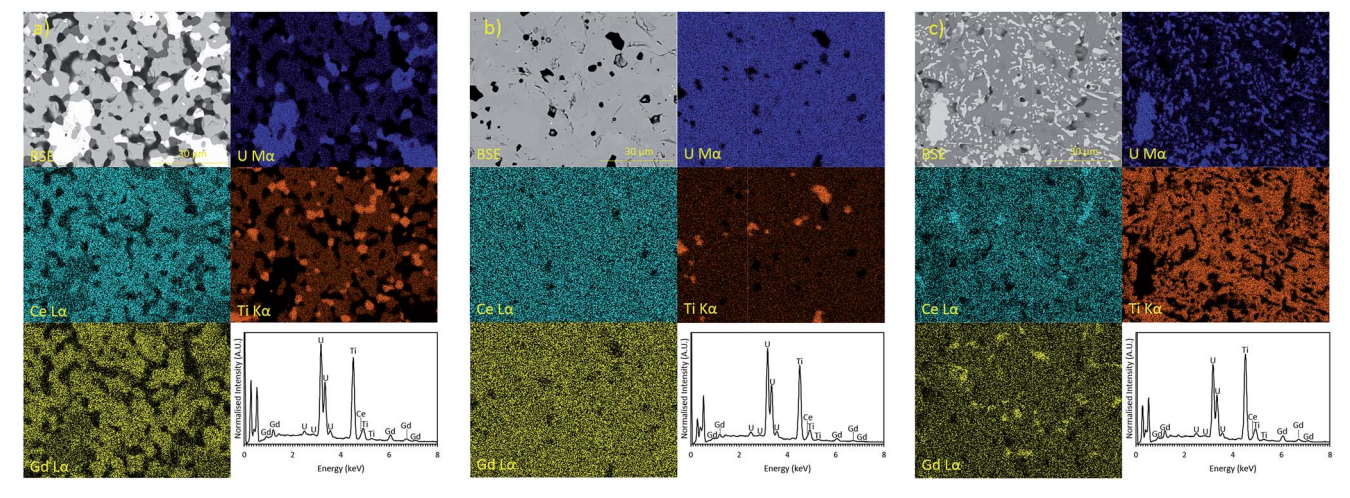


Fig. 3 EDX spectra and elemental partitioning observed in  $Gd_{0.1}U_{0.81}Ce_{0.09}Ti_2O_6$  synthesised in: (a) air; (b) Argon and (c) 5%  $H_2/N_2$ .

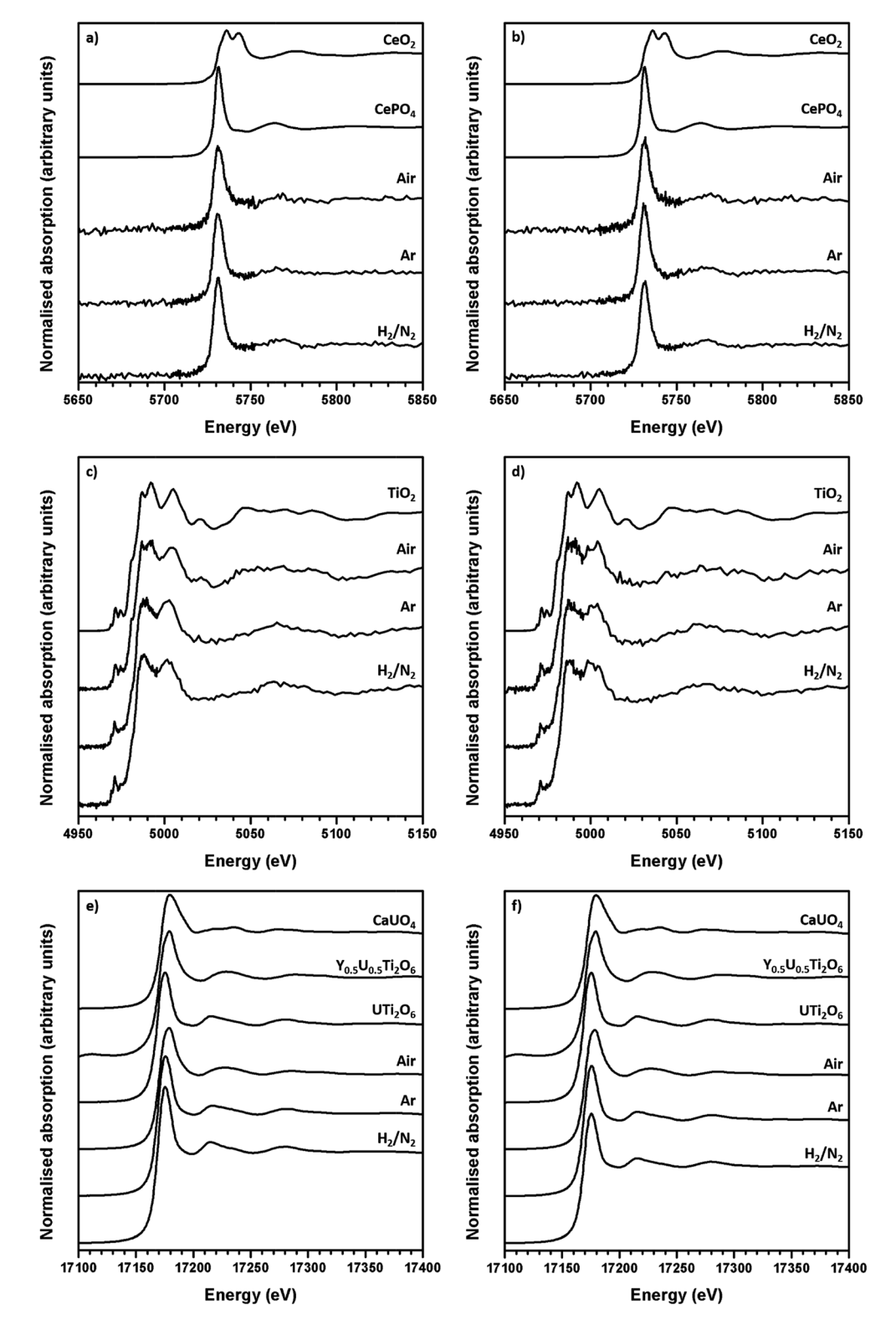


Fig. 4 Representative XANES spectra of synthesised brannerites. (a) Ce  $L_{III}$  edge  $Gd_{0.1}U_{0.81}Ce_{0.1}Ti_2O_6$ ; (b)  $Ce L_{III}$  edge  $Ca_{0.1}Gd_{0.1}U_{0.72}Ce_{0.08}Ti_2O_6$ ; (c) Ti K edge  $Gd_{0.1}U_{0.81}Ce_{0.1}Ti_2O_6$  and (d) Ti K edge  $Ca_{0.1}Gd_{0.1}U_{0.72}Ce_{0.08}Ti_2O_6$ ; (e) U  $L_{III}$  edge  $Gd_{0.1}U_{0.81}Ce_{0.1}Ti_2O_6$  and (f) U  $L_{III}$  edge  $Ca_{0.1}Gd_{0.1}U_{0.72}Ce_{0.08}Ti_2O_6$ .

Heat treatment of samples in a 5%  $\rm H_2/N_2$  atmosphere was found to result in the formation of brannerite, pyrochlore and a rare earth titanate phase along with the retention of  $\rm UO_2$  throughout the samples.

From EDX analysis, it is evident that Gd and Ce are preferentially incorporated in the brannerite phase when samples are produced in an oxidising environment, Fig. 3a. Increased substitution of Gd may lead to the formation of single phase

Paper RSC Advances

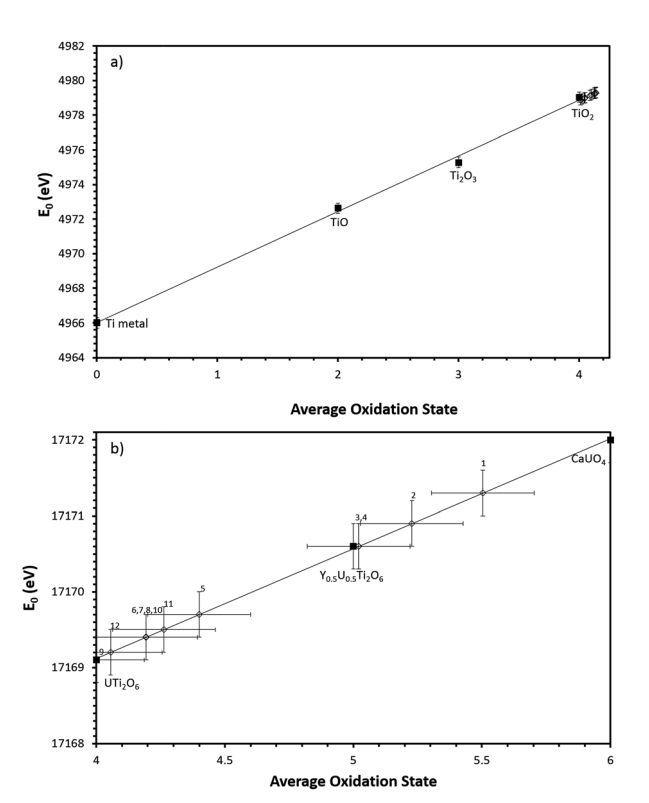


Fig. 5 (a) Linear regression of Ti K edge  $E_0$  values with respect to Ti standards. (b) Linear regression of U L-III edge  $E_0$  values with respect to U standards. Numbers refer to corresponding composition no. in Table 2. Black squares denote standards, open diamonds denote samples.

brannerite, however, the level of substitution required to achieve the desired phase assemblage would have a negative impact on the waste loading of a final wasteform.

Samples produced in an Ar atmosphere were found to exhibit different partitioning behaviour; as can be seen in Fig. 3b, Gd is clearly enriched in the pyrochlore phase and Ti is enriched in the rutile phase. Cerium does not clearly partition to either the brannerite or pyrochlore phase. However, the removal of Gd from the brannerite by the parasitic formation of pyrochlore may have a negative impact on the criticality performance of a final wasteform.

Samples synthesised in a reducing 5%  $\rm H_2/N_2$  atmosphere, Fig. 3c, exhibited similar elemental partitioning to those synthesised in an Ar atmosphere however; it is clear that a greater proportion of the U inventory is retained as  $\rm UO_2$ . Although there is some local enrichment visible in the EDX map, Ce does not show clear partitioning into any one phase.

#### 3.3 Bulk X-ray absorption spectroscopy

The average oxidation state of Ti, Ce and U in the synthesised brannerites were determined by X-ray absorption spectroscopy near edge spectroscopy (XANES). Fig. 4 shows representative Ce L-III, Ti K and U L-III edge XANES data.

Ti K-edge XANES data show that the predominant oxidation state of Ti in all samples is  ${\rm Ti}^{4+}$ , see Fig. 4c, d and 5a, as the white line positions ( $E_0=4979.0\pm0.3~{\rm eV}$ ) and pre-edge features are similar in character to the TiO<sub>2</sub> standard.

**Table 2** Average U oxidation state of synthesised brannerites as determined by linear regression with respect to standards

Sample no.	Nominal composition	Atmosphere	Oxidation state
1	Gd <sub>0.1</sub> U <sub>0.81</sub> Ce <sub>0.09</sub> Ti <sub>2</sub> O <sub>6</sub>	Air	5.5 (±0.2)
2	Gd <sub>0.2</sub> U <sub>0.72</sub> Ce <sub>0.08</sub> Ti <sub>2</sub> O <sub>6</sub>	Air	$5.2 (\pm 0.2)$
3	Gd <sub>0.25</sub> U <sub>0.675</sub> Ce <sub>0.075</sub> Ti <sub>2</sub> O <sub>6</sub>	Air	$5.0\ (\pm0.2)$
4	Ca <sub>0.1</sub> Gd <sub>0.1</sub> U <sub>0.72</sub> Ce <sub>0.08</sub> Ti <sub>2</sub> O <sub>6</sub>	Air	$5.0\ (\pm0.2)$
5	$Gd_{0.1}U_{0.81}Ce_{0.09}Ti_2O_6$	Ar	$4.4\ (\pm0.2)$
6	$Gd_{0.2}U_{0.72}Ce_{0.08}Ti_2O_6$	Ar	$4.2\ (\pm0.2)$
7	$Gd_{0.25}U_{0.675}Ce_{0.075}Ti_2O_6$	Ar	$4.2~(\pm 0.2)$
8	$Ca_{0.1}Gd_{0.1}U_{0.72}Ce_{0.08}Ti_2O_6$	Ar	$4.2~(\pm 0.2)$
9	$Gd_{0.1}U_{0.81}Ce_{0.09}Ti_2O_6$	$5\% \ H_2/N_2$	$4.0~(\pm 0.2)$
10	$Gd_{0.2}U_{0.72}Ce_{0.08}Ti_2O_6$	$5\% H_2/N_2$	$4.2~(\pm 0.2)$
11	$Gd_{0.25}U_{0.675}Ce_{0.075}Ti_2O_6$	$5\% \ H_2/N_2$	$4.3\ (\pm0.2)$
12	$Ca_{0.1}Gd_{0.1}U_{0.72}Ce_{0.08}Ti_{2}O_{6}$	$5\%~\mathrm{H_2/N_2}$	$4.1~(\pm 0.2)$

This indicates that the oxidation state of Ti remains unchanged relative to the initial TiO<sub>2</sub> precursor and is insensitive to both composition and processing atmosphere.

Ce L-III edge XANES data show that the position of the absorption edge and post-edge oscillations of Ce in synthesised brannerites are similar in character to the CePO<sub>4</sub> standard (5725.0 eV). This indicates that the cerium has been reduced from Ce<sup>4+</sup> to Ce<sup>3+</sup> during synthesis. As can be seen, this reduction occurs regardless of processing atmosphere or composition and it is consistent with results of previous studies involving the substitution of Ce into the brannerite structure.<sup>13,17</sup>

As the Ti and Ce XANES data show, the oxidation states of Ce and Ti in the synthesised brannerites are insensitive to both processing atmosphere and stoichiometry. In contrast, it was found that the average U oxidation state was strongly affected by the processing atmosphere.

Samples synthesised in air exhibited an absorption edge and post-edge oscillations indicative of a mixed U<sup>5+/6+</sup> oxidation

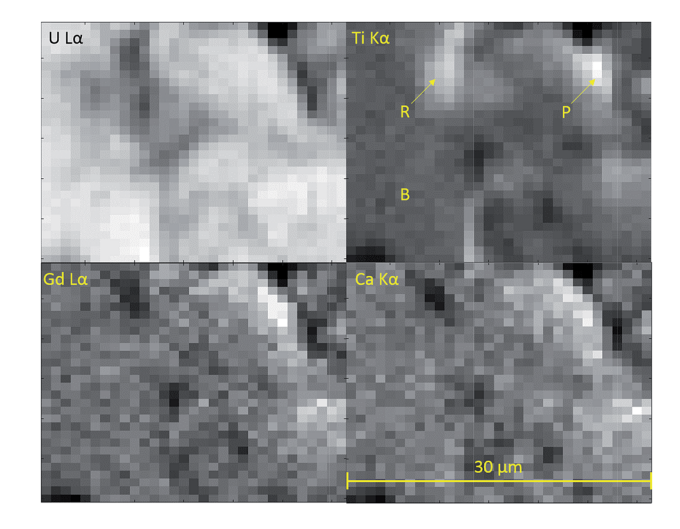


Fig. 6 Fluorescence maps of  $Ca_{0.1}Gd_{0.1}U_{0.72}Ce_{0.08}Ti_2O_6$  sintered in an argon atmosphere. Each pixel represents 1  $\mu$ m². Lighter colours indicate higher X-ray fluorescence intensity, darker colours indicate lower intensity. B-brannerite, P-pyrochlore and R-rutile.

**RSC Advances** 

Table 3 Oxidation state of uranium in the brannerite phase as found by micro-focus XAS and linear regression with respect to standards

Sample no.	Nominal composition	Atmosphere	Oxidation state
1	Gd <sub>0.1</sub> U <sub>0.81</sub> Ce <sub>0.09</sub> Ti <sub>2</sub> O <sub>6</sub>	Air	5.0 (±0.2)
2	$Gd_{0.2}U_{0.72}Ce_{0.08}Ti_2O_6$	Air	$4.6\ (\pm0.2)$
3	Gd <sub>0.25</sub> U <sub>0.675</sub> Ce <sub>0.075</sub> Ti <sub>2</sub> O <sub>6</sub>	Air	$4.6\ (\pm0.2)$
4	$Ca_{0.1}Gd_{0.1}U_{0.72}Ce_{0.08}Ti_2O_6$	Air	$5.2\ (\pm0.2)$
5	$Gd_{0.1}U_{0.81}Ce_{0.09}Ti_2O_6$	Ar	$4.5\ (\pm0.2)$
6	$Gd_{0.2}U_{0.72}Ce_{0.08}Ti_2O_6$	Ar	$4.5\ (\pm0.2)$
7	$Gd_{0.25}U_{0.675}Ce_{0.075}Ti_{2}O_{6}$	Ar	$4.5\ (\pm0.2)$
8	Ca <sub>0.1</sub> Gd <sub>0.1</sub> U <sub>0.72</sub> Ce <sub>0.08</sub> Ti <sub>2</sub> O <sub>6</sub>	Ar	$4.6~(\pm 0.2)$
9	$Gd_{0.1}U_{0.81}Ce_{0.09}Ti_2O_6$	$5\% \text{ H}_2/\text{N}_2$	$4.4\ (\pm0.2)$
10	$Gd_{0.2}U_{0.72}Ce_{0.08}Ti_2O_6$	$5\% H_2/N_2$	$4.1~(\pm 0.2)$
11	$Gd_{0.25}U_{0.675}Ce_{0.075}Ti_{2}O_{6}$	$5\% \ H_2/N_2$	$4.5\ (\pm0.2)$
12	$Ca_{0.1}Gd_{0.1}U_{0.72}Ce_{0.08}Ti_{2}O_{6}$	$5\%~\mathrm{H_2/N_2}$	$4.4\ (\pm0.2)$

state whereas samples synthesised under Ar or 5% H<sub>2</sub>/N<sub>2</sub> possessed features indicative of mixed U<sup>4+/5+</sup> oxidation states. Table 2 shows the average U oxidation state for the synthesised brannerites, as determined by linear regression with respect to standards (Fig. 5b). It is clear that processing atmosphere has a strong influence on the average oxidation state of U. However, comparison between different compositions processed in the same atmosphere does not reveal a strong compositional influence.

The presence of minor U-bearing accessory phases such as U<sub>3</sub>O<sub>8</sub> and UO<sub>2</sub> means that, although indicative, the bulk U oxidation state is not representative of the oxidation state of U in the brannerite phase. As a result, the oxidation state of U in the brannerite phase was subject to further investigation by micro-focus XAS.

#### Micro-focus X-ray absorption spectroscopy

Micro-focus X-ray spectroscopy was used to determine the oxidation state of U in the brannerite phase. XRF maps were

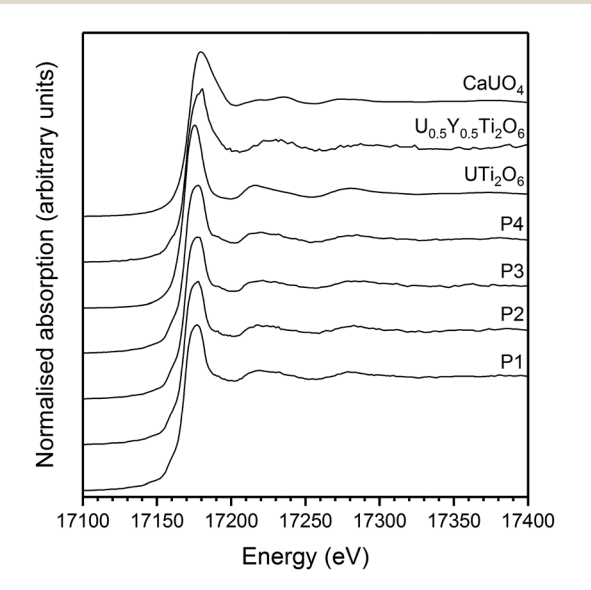


Fig. 7 Example U L-III edge  $\mu$ -focus XANES for  $Gd_{0.1}U_{0.81}Ce_{0.09}Ti_2O_6$ synthesised in argon. P1-4 indicate individual spectra taken from separate points.

Table 4 Comparison of nominal composition and determined average composition of brannerites synthesised in argon atmosphere

Nominal composition	Determined average composition		
$Gd_{0.1}U_{0.81}Ce_{0.09}Ti_{2}O_{6}$	$\big(Gd_{0.09\pm0.01}U_{0.76\pm0.04}Ce_{0.04\pm0.01}$		
Gd <sub>0.2</sub> U <sub>0.72</sub> Ce <sub>0.08</sub> Ti <sub>2</sub> O <sub>6</sub>	$\text{Ti}_{0.04\pm0.03}\Box_{0.07}\text{)}\text{Ti}_{2.00\pm0.03}\text{O}_{6} \ (\text{Gd}_{0.17\pm0.01}\text{U}_{0.71\pm0.03}\text{Ce}_{0.05\pm0.01}$		
340.200.72300.0811236	$\text{Ti}_{0.04\pm0.03}\Box_{0.03}\text{Ti}_{2.00\pm0.03}\text{O}_{6}$		
$Gd_{0.25}U_{0.675}Ce_{0.075}Ti_2O_6$	$(\mathrm{Gd}_{0.21\pm0.03}\mathrm{U}_{0.66\pm0.03}\mathrm{Ce}_{0.04\pm0.01}\ \mathrm{Ti}_{0.06\pm0.06}\square_{0.03})\mathrm{Ti}_{2.00\pm0.06}\mathrm{O}_{6}$		
$Ca_{0.1}Gd_{0.1}U_{0.72}Ce_{0.08}Ti_{2}O_{6}$	$(Ca_{0.02\pm0.06}\Box_{0.03}^{-112.00\pm0.06}U_{0.79\pm0.02}^{-10.06}U_{0$		
	$Ce_{0.03\pm0.01}\square_{0.07})Ti_{2.00\pm0.05}O_6$		

used to determine which regions of the sample were brannerite and which were secondary phases, example maps are shown in Fig. 6. Rutile and pyrochlore phases were easily distinguished by a strong Ti Kα emission, together with Gd Lα or Ca Lα emission respectively. U<sub>3</sub>O<sub>8</sub> and UO<sub>2</sub> were distinguished by the absence of Gd Lα, Ca Lα and Ti Kα emission.

U oxidation states, as determined by linear regression with respect to standards, are given in Table 3. Example micro-focus spectra are shown in Fig. 7. A general trend may be observed when comparing the effect of processing atmosphere on the U oxidation state; samples sintered in air had the highest U oxidation state, samples sintered in a reducing atmosphere had the lowest; and samples produced in inert conditions were intermediate between the two extremes. The oxidation of U to higher oxidation states was expected in order to compensate for the incorporation of Ca, Ce and Gd and is in agreement with the results reported by Vance et al.4 The relatively high oxidation state observed in samples sintered in air may be explained by the large amount of U<sub>3</sub>O<sub>8</sub> present in the bulk of the sample: as Gd is incorporated in the brannerite phase and a substantial amount of U is incorporated in U<sub>3</sub>O<sub>8</sub>, the relative proportion of Gd to U in the brannerite phase is higher than in the target composition; consequently, U contained within the brannerite phase must oxidise further to compensate for the relative increase in Gd concentration.

#### Charge balance mechanism

Combining the results of microfocus XANES with those of SEM-EDX and bulk XANES, a credible charge balance mechanism was derived. Assuming that oxygen is fully stoichiometric, the Asite is cation deficient and incorporates a small proportion of Ti. The charge balance mechanism is therefore hypothesised to be a combination of A-site vacancies and the oxidation of U<sup>4+</sup> to higher oxidation states. Assuming this charge balance mechanism, the average composition closely follows that of the nominal, batched composition (Table 4) and is consistent with the secondary phases observed by SEM-EDX.

#### Conclusions

Brannerite compositions have been synthesised under oxidising, inert and reducing atmospheres. Characterisation by XRD and SEM-EDX has shown that the final phase assemblage and

**RSC Advances** Paper

elemental partitioning of brannerite wasteforms is affected by both processing atmosphere and stoichiometry. The most favourable phase assemblages were produced processing in an argon atmosphere. Increasing substitution of Gd and Ca was found to have a negative impact on the resultant phase assemblage of samples produced in inert atmospheres. The most favourable phase assemblage was produced for the target stoichiometry Gd<sub>0.1</sub>U<sub>0.81</sub>Ce<sub>0.09</sub>Ti<sub>2</sub>O<sub>6</sub> when sintered in argon. Under these conditions Ce was incorporated into the brannerite phase indicating a promising route for immobilisation of expected MOX residue compositions. As the MOX compositions investigated in this study were at the upper bounds of expected Pu concentration for light water reactor fuels, it would be reasonable to assume that immobilisation of lower concentrations of Pu would not result in significant deviation from the outcomes of this study. Combined bulk and micro-focus XANES have established the oxidation states of Ti, Ce and U in synthesised brannerites. Combination of XANES and SEM-EDX data indicates a charge balance mechanism that uses a combination of U oxidation and A-site vacancies to achieve charge neutrality. It is clear that, in order to produce an optimised wasteform, careful consideration must be given to both the processing conditions and system stoichiometry.

#### Conflicts of interest

There are no conflicts of interest to declare.

### Acknowledgements

UK EPSRC is thanked for providing studentship and fellowship for DJB through the Nuclear FiRST Doctoral Training Centre and EPSRC Doctoral Prize Fellowship (Grant EP/G037140/1, EP/ M026566/1 and EP/R512175/1). Use of the National Synchrotron Light Source, Brookhaven National Laboratory, was supported by the U.S. Department of Energy, Office of Science, Office of Basic Energy Sciences, under Contract No. DE-AC02-98CH10886. Access to the Swiss Light Source, Paul Scherrer Institute, Villigen, Switzerland, was supported by the TALISMAN collaborative project, with co-funding from the European Commission under the Euratom Research and Training Programme on Nuclear Energy, within the 7<sup>th</sup> Framework programme (grant agreement 323300). NCH is grateful to

the Royal Academy of Engineering and Nuclear Decommissioning Authority for funding. We thank Hands on Thin Sections Ltd. for preparation of the thin section specimens. This research was performed in part at the MIDAS Facility, at the University of Sheffield, which was established with support from the Department of Energy and Climate Change.

#### Notes and references

- 1 Nuclear Decomissioning Authority, Progress on approaches to the management of separated plutonium, 2014.
- 2 N. C. Hyatt, Energy Policy, 2017, 101, 303-309.
- 3 J. T. Szymanski and J. D. Scott, Can. Mineral., 1982, 20, 271-279.
- 4 E. R. Vance, J. N. Watson, M. L. Carter, R. A. Day and B. D. Begg, I. Am. Ceram. Soc., 2001, 44, 141-144.
- 5 M. James and J. N. Watson, J. Solid State Chem., 2002, 165, 261-265.
- 6 F. X. Zhang, M. Lang, Z. Liu and R. C. Ewing, J. Solid State Chem., 2011, 184, 2834-2839.
- 7 G. R. Lumpkin, J. Nucl. Mater., 2001, 289, 136-166.
- 8 Y. Zhang, G. R. Lumpkin, H. Li, M. G. Blackford, M. Colella, M. L. Carter and E. R. Vance, J. Nucl. Mater., 2006, 350, 293-300.
- 9 M. C. Stennett, C. L. Freeman, A. S. Gandy and N. C. Hyatt, J. Solid State Chem., 2012, 192, 172-178.
- 10 J. E. Patchettt and E. W. Nuffield, Can. Mineral., 1960, 6, 483-490.
- 11 M. James, M. L. Carter and J. N. Watson, J. Solid State Chem., 2003, 174, 329-333.
- 12 D. J. Bailey, M. C. Stennett and N. C. Hyatt, Procedia Chem., 2016, 21, 371-377.
- 13 D. J. Bailey, M. C. Stennett and N. C. Hyatt, MRS Adv., 2016, 2, 557-562.
- 14 P. D. Wilson, The Nuclear Fuel Cycle: From Ore to Waste, Oxford University Press, Oxford, 1st edn, 1996.
- 15 B. Ravel and M. Newville, J. Synchrotron Radiat., 2005, 12, 537-541.
- 16 B. Ravel and M. Newville, Phys. Scr., 2005, 1007.
- 17 S. V. Stefanovsky, S. V. Yudintsev, A. A. Shiryaev, V. Y. Murzin and A. L. Trigub, J. Eur. Ceram. Soc., 2017, 37, 771-777.